Nuclear Engineering and Technology 55 (2023) 2935–2940

Contents lists available at ScienceDirect

Nuclear Engineering and Technology

journal homepage: www.elsevier.com/locate/net

Original Article

Development of a polystyrene phantom for quality assurance of a Gamma Knife®

Yona Choi [a], Kook Jin Chun [a], Jungbae Bahng [a], Sang Hyoun Choi [b], Gyu Seok Cho [b], Tae Hoon Kim [c], Hye Jeong Yang [d], Yeong Chan Seo [e], Hyun-Tai Chung [e, f, *]

[a] Department of Accelerator Sciences, Korea University Sejong Campus, Sejong, South Korea
[b] Department of Research Team of Radiological Physics and Engineering, Korea Institute of Radiological and Medical Sciences, Seoul, South Korea
[c] Department of Radiation Oncology, Asan Medical Center, Seoul, South Korea
[d] Department of Proton Therapy Center, National Cancer Center, Goyang, South Korea
[e] Department of Medical Device Development, Seoul National University College of Medicine, Seoul, South Korea
[f] Department of Neurosurgery, Seoul National University Hospital, Seoul, South Korea

ARTICLE INFO

Article history:
Received 4 October 2022
Received in revised form
13 April 2023
Accepted 19 April 2023
Available online 19 June 2023

Keywords:
Leksell Gamma Knife
Polystyrene phantom
Absorbed dose rate to water
Dose distribution
Machine-specific reference correction

ABSTRACT

A polystyrene phantom was developed following the guidance of the International Atomic Energy Association (IAEA) for gamma knife (GK) quality assurance. Its performance was assessed by measuring the absorbed dose rate to water and dose distributions. The phantom was made of polystyrene, which has an electron density (1.0156) similar to that of water. The phantom included one outer phantom and four inner phantoms. Two inner phantoms held PTW T31010 and Exradin A16 ion chambers. One inner phantom held a film in the XY plane of the Leksell coordinate system, and another inner phantom held a film in the YZ or ZX planes. The absorbed dose rate to water and beam profiles of the machine-specific reference (msr) field, namely, the 16 mm collimator field of a GK Perfexion™ or Icon™, were measured at seven GK sites. The measured results were compared to those of an IAEA-recommended solid water (SW) phantom. The radius of the polystyrene phantom was determined to be 7.88 cm by converting the electron density of the plastic, considering a water depth of 8 g/cm^2. The absorbed dose rates to water measured in both phantoms differed from the treatment planning program by less than 1.1%. Before msr correction, the PTW T31010 dose rates (PTW Freiberg GmbH, New York, NY, USA) in the polystyrene phantom were 0.70 (0.29)% higher on average than those in the SW phantom. The Exradin A16 (Standard Imaging, Middleton, WI, USA) dose rates were 0.76 (0.32)% higher in the polystyrene phantom. After msr correction factors were applied, there were no statistically significant differences in the A16 dose rates measured in the two phantoms; however, the T31010 dose rates were 0.72 (0.29)% higher in the polystyrene phantom. When the full widths at half maximum and penumbras of the msr field were compared, no significant differences between the two phantoms were observed, except for the penumbra in the Y-axis. However, the difference in the penumbra was smaller than variations among different sites. A polystyrene phantom developed for gamma knife dosimetry showed dosimetric performance comparable to that of a commercial SW phantom. In addition to its cost effectiveness, the polystyrene phantom removes air space around the detector. Additional simulations of the msr correction factors of the polystyrene phantom should be performed.

1. Introduction

A Gamma Knife® (GK; Elekta AB, Stockholm, Sweden) is a stereotactic radiosurgery device that treats intracranial lesions using ^{60}Co sources [1]. Because GKs deliver a considerable amount of radiation to patients in single or multiple sessions, verifying the dose rate and distribution is critical. Several researchers have employed water-filled phantoms to measure the absorbed dose to water at the center of a GK [2,3]. However, to ensure that the phantom does not break inside the machine, plastic phantoms have been used for quality assurance. The International Atomic Energy

* Corresponding author. Department of Medical Device Development, Seoul National University College of Medicine, Seoul, South Korea.
E-mail address: htchung@snu.ac.kr (H.-T. Chung).

https://doi.org/10.1016/j.net.2023.04.031

Agency (IAEA) and American Association of Physicists in Medicine (AAPM) recommended using plastic phantoms in their codes of practice, TRS-483 [4] and TG-178 [5]. Two types of plastic phantoms are available to GK users. An acrylonitrile butadiene styrene (ABS) phantom is an eight cm radius sphere that was mainly used for earlier GK models, including Type U™, Type B™, and Type C™. However, the holder for fixing ABS phantoms to Perfexion/Icon models blocks some ^{60}Co beams [6]. A solid water (SW, Gamex Model 457, SUN NUCLEAR Co., Melbourne, FL, USA) phantom is also an 8 cm radius sphere that was introduced for later models, such as Perfexion™ and Icon™. The solid water phantom is preferred over the previous model because its physical density (1.04 g/cm^3) is close to that of water, and SW phantoms have shown good performance in GK quality assurance [7]. The LUCY® 3D QA phantom (Standard Imaging, Inc. Middleton, WI, USA) with proper tools has also been used for GK maintenance [8].

Some practical problems with commercial phantoms for GKs include their high costs and rigidity in applications. Phantoms have high costs, and users must purchase different detector inserts for each type of detector model because the insertion part is tailored to the detector structure. A spherical PMMA phantom was developed for GK dosimetry to replace commercial phantoms [9]. The dose rate measured in the PMMA phantom was 1.8% higher than that measured in an SW phantom. Moreover, compared with the SW phantom, the full widths at half maximum (FWHMs) along the three axes of the Leksell stereotactic coordinate system obtained with the PMMA phantom were within experimental uncertainties. However, the penumbras, which are defined as the distance between the 80% dose point and 20% dose point, were broader than those measured in SW phantoms because the 20% dose widths were thicker in the PMMA phantom. The authors attributed the higher dose rate and wider 20% dose width to scattered photons in the phantom. The electron density of PMMA is 1.155 times higher than the electron density of water. Thus, although the radius of the PMMA phantom was determined to be 6.93 cm, considering the higher electron density, the scattered photons contributed more than expected. Thus, the authors developed a new spherical phantom made of polystyrene and assessed its dosimetric features in this study. Because the electron density of the polystyrene used in this study was 1.0156 times greater than that of water, the results were more consistent with the SW phantom results. The phantom proposed in this study has several advantages. The air space near the ion chamber in the SW phantom was reduced, and the ion chamber could be tightly attached with a holder. In addition, users could verify the position of the detector inside the phantom because the phantom was transparent.

2. Materials & methods

2.1. Polystyrene phantom

Polystyrene is one of the plastics recommended by IAEA TRS-483 as a phantom material because of several advantages, such as having an electron density similar to that of water [4]. The physical and chemical characteristics of the polystyrene used in this study were analyzed at the Korea Research Institute of Chemical Technology. The mass density was 1.0460 ± 0.0009 g/cm^3, which was determined by measuring the mass and size of two samples ten times. The composition ratio was analyzed through elemental analysis (Table 1). The electron density of the polystyrene was obtained by summing the electron densities of each component, as shown in Eq. (1).where ρ_{PS}^{mass} is the mass density of the polystyrene, f_i is the weight fraction of the i_{th} element, and $\left(\frac{Z}{A}\right)_i$ is the atomic number to atomic weight ratio [10]. The water equivalent radius of

Table 1
This chemical composition and electron density of the polystyrene used in this study.

$$\rho_{PS}^{el} = \rho_{PS}^{mass} \times \left[\sum_i f_i \left(\frac{Z}{A}\right)_i\right] \quad (1)$$

Component	f_i	$(Z/A)_i$	ρ_i^{el} (N$_e$/mol)	ρ_{PS}^{el} (N$_e$/mol)	$\rho_{PS}^{el}/\rho_{H_2O}^{el}$
C	0.91932	0.49954	0.48039	0.56258	1.0156
H	0.07769	0.99216	0.08062		
O	0.00199	0.50003	0.00104		
N	0.00100	0.49975	0.00052		

the polystyrene (r_{PS}) was determined by dividing the water radius (r_W) by the electron density ratio (Eq. (2)) [10].

$$r_{PS} = r_W \frac{\rho_{H_2O}^{el}}{\rho_{PS}^{el}} \quad (2)$$

where $\rho_{H_2O}^{el}$ is the electron density of water and ρ_{PS}^{el} is the electron density of polystyrene. The relative electron density of the polystyrene was 1.0156; thus, the polystyrene radius corresponding to the 8.00 cm water radius was 7.88 cm.

The phantom consisted of one outer phantom and four inner phantoms (Fig. 1). Two inner phantoms held PTW T31010 (PTW Freiberg GmbH, New York, NY, USA) and Exradin A16 (Standard Imaging, Middleton, WI, USA) ion chambers. One inner phantom held a film in the XY plane of the Leksell coordinate system, and the other inner phantom held a film in the YZ or ZX planes. The X-axis is set from the right to left sides of the patient, the Y-axis is set from back to front, and the Z-axis is set from the head to the feet. The bottom of the outer phantom was manufactured to ensure that the phantom could be fixed to a Leksell G-frame with screws (Fig. 1e). A cable holder was used to stabilize the ion chamber (Fig. 1f). The machining tolerance was 0.05 mm. The inner phantoms were attached to the outer phantom with the smallest possible air gap to

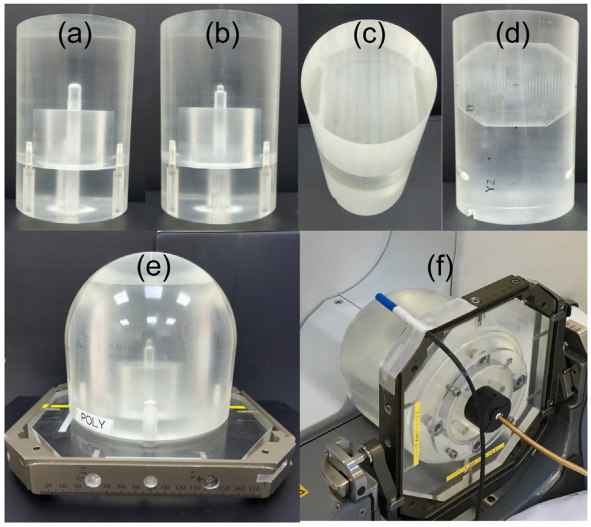

Fig. 1. The inner phantom for PTW T31010 (a) and Exradin A16 (b). The XY plane film holder (c) and YZ or ZX plane film holder (d). The outer phantom with an Exradin A16 inner holder was attached to a Leksell G-frame (e). The phantom was set on a Gamma Knife (f). The blue cylinder is a thermosensor, and the black cylinder at the bottom of the phantom is an ion chamber cable holder. (For interpretation of the references to colour in this figure legend, the reader is referred to the Web version of this article.)

allow the entire phantom to be approximated as homogenous. Direction guides on each phantom were applied to ensure the correct orientations.

2.2. Dose rate measurement

The absorbed dose rate to water of the machine-specific reference (msr) field, namely, the 16 mm collimator field of a GK Perfexion™ or Icon™, was measured at seven GK sites, including Icon™ sites and two Perfexion™ sites. The PTW T31010 or Exradin A16 ion chamber was set at the center of the SW or polystyrene phantom. The active point of the ion chamber was located at the unit center point (UCP, X = Y = Z = 100.0) of the GK. The ion chambers were calibrated following the IAEA TRS-398 protocol at a Secondary Standard Dosimetry Laboratory (SSDL) at the Korea Institute of Radiological and Medical Sciences (KIRAMS) according to the International Bureau of Weights and Measures. An Unidos-Webline electrometer (PTW Freiberg GmbH, New York, NY, USA) was used to calibrate the ion chambers and collect the charges. An F250 precision thermometer (Automatic Systems Laboratories, Croydon, UK) and Mensor 2105 precision barometer (MENSOR Corp, San Marcos, USA) were used to measure the temperature and pressure in real time. Each measurement set included ten consecutive charge recordings over 1 min, as well as the temperature and air pressure for each ion chamber/phantom combination. The experiments were performed by a single team using the same set of devices. The chamber and phantom were placed in the GK room at least one and half hours before measurements, and the ion chambers were pre-irradiated with 10–12 Gy. The location of the detector's active point was verified using cone beam computed tomography (CBCT) of the GK Icon™ when available.

The dose rates were determined following the IAEA TRS-483 protocol, which is equivalent to AAPM TG-178, as shown in Eq. (3).

$$D^{f_{msr}}_{W,Q_{msr}} = M^{f_{msr}}_{Q_{msr}} N^{f_{ref}}_{D,W,Q_0} k^{f_{msr},f_{ref}}_{Q_{msr},Q_0} \quad (3)$$

where $M^{f_{msr}}_{Q_{msr}}$ is the ion chamber reading after the necessary corrections to the msr field were applied, $N^{f_{ref}}_{D,W,Q_0}$ is the calibration coefficient determined at a standard laboratory, and $k^{f_{msr},f_{ref}}_{Q_{msr},Q_0}$ is the msr correction factor. The indices of f_{ref}, Q_0, f_{msr} and Q_{msr} denote the reference field, beam quality at the reference field, msr field, and beam quality at the msr field, respectively.

Several studies have reported the msr correction factors for Icon/Perfexion GKs, as shown in Table 2. The average values of the msr correction factors were used in this study because they provided the most consistent dose rates with an SW phantom in a separate study [11]. IAEA TRS-483 recommends using a plastic thickness equivalent to the water depth in the msr field. However, this protocol provides the msr correction factors for 8 cm radius plastic phantoms instead of water equivalent depths. Two previous studies reported msr correction factors for polystyrene phantoms, and they also used an 8 cm radius [12,15]. The authors assumed that the errors introduced by using the reported msr correction factors for this study's polystyrene phantom could be neglected because the radius differed by only 0.12 cm.

2.3. Dose profile measurement

The FWHM and penumbra of the msr field were measured using GafChromic™ EBT3 films (Ashland, Covington, KY) in the SW and polystyrene phantoms. The film was measured followed standard procedures [16]. The films were calibrated by irradiating the films with fifteen doses ranging from 0.5 to 10.0 Gy in steps of 0.5 or 1.0 Gy. Three films were irradiated at each dose, and the mean optical density was used. The films were scanned one week after irradiation using an EPSON Expression 12000XL scanner (Seiko-Epson Co, Nagano, Japan) with 300 DPI resolution. The red channel values were fitted with a third-order polynomial to convert the optical density to the absorbed dose using the commercial software Origin 2019 (OriginLab Corp, Northampton, MA, USA). The film measurements were performed at seven GK sites. The dose distributions in the XY and ZX planes were obtained for both phantoms at each site. The absorbed dose profiles were analyzed using DoseLab version 6.80 (Mobius Co, Houston, USA) software. Three films were irradiated in each plane, and the mean values were used in the analyses.

2.4. Statistical analyses

Statistical analyses were performed using IBM SPSS software version 25. The normality of the data was evaluated with Kolmogorov–Smirnov tests. Wilcoxon signed-rank tests were used to compare paired groups. The values in parentheses indicate the experimental standard deviations unless otherwise specified.

3. Results

3.1. Polystyrene phantom

The active point in the ion chamber was verified with CBCT, and Fig. 2a to c shows an example of the A16 chamber, where the active point was located at (99.9, 100.1, 100.0). Three-dimensional dislocations of the T31010 and A16 chambers were 0.2 (0.1) mm in both phantoms, which are comparable to the dislocations of the UCP of the seven GKs obtained in annual management procedures. The film holder configuration was also assessed with CBCT, as shown in Fig. 2d to f.

3.2. Absorbed dose rate to water

As shown in Table 3, the absorbed dose rates to water measured in both phantoms differed from the treatment planning program by

Table 2
The machine-specific reference correction factors for the three ion chambers used in this study. An ion chamber was placed at the center of a phantom in the 16 mm collimator field of a Gamma Knife Perfexion or Icon. The numbers in parentheses indicate the standard uncertainties of each method ($k = 1$).

Phantom	Chamber	TRS-483[4]	Mirzak[12]	Zoros[13]	Schaarschmidt[14,15]			Average
					S.Pen[a]	S.Opt3[a]	S.Opt4[a]	
Solid water	T31010	1.0037 (0.0020)	1.0093 (0.0045)	1.008 (0.004)	0.997 (0.004)	1.000 (0.006)	1.005 (0.006)	1.004 (0.005)
	A16	1.0167 (0.0020)	1.0211 (0.0046)	1.023 (0.004)	1.010 (0.007)	1.023 (0.011)	1.017 (0.011)	1.018 (0.007)
Poly-styrene	T31010	–	1.0135 (0.0046)	–	1.000 (0.004)	0.998 (0.006)	1.005 (0.006)	1.004 (0.007)
	A16	–	1.0244 (0.0046)	–	1.006 (0.007)	1.011 (0.011)	1.003 (0.011)	1.011 (0.009)

[a] Physics model was Penelope (S.Pen), Standard Option 3 (S.Opt3), and Standard Option 4 (S.Opt4) in Geant 4 simulations.

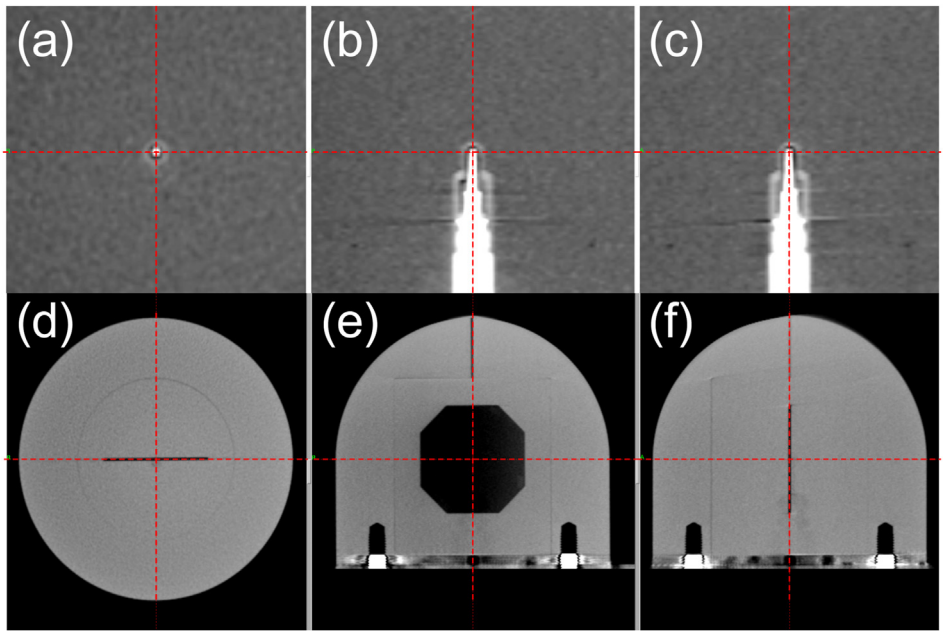

Fig. 2. Cone beam CT images of an Exradin A16 ion chamber (a: axial, b: coronal, c: sagittal) and a film holder in the ZX plane (d: axial, e: coronal, f: sagittal) in the polystyrene phantom. The cross point of the red dotted lines in the upper images corresponds to the active point in the chamber, and its coordinates are (99.9, 100.1, 100.0) in this case. The red dotted lines in the lower images correspond to the X-, Y-, and Z-axes in the Leksell coordinate system. (For interpretation of the references to colour in this figure legend, the reader is referred to the Web version of this article.)

Table 3
Absorbed dose rates measured with the two ion chambers in the two plastic phantoms. The values before applying machine-specific reference correction factors are also provided.

		Before msr correction				After msr correction			
		T31010		A16		T31010		A16	
Site	LGP	SW	PS	SW	PS	SW	PS	SW	PS
1	1.783	1.786	1.798	1.765	1.781	1.793	1.806	1.798	1.800
2	2.094	2.071	2.089	2.039	2.057	2.079	2.097	2.077	2.079
3	2.427	2.424	2.438	2.383	2.408	2.433	2.448	2.427	2.435
4	2.142	2.131	2.143	2.100	2.109	2.139	2.152	2.138	2.133
5	1.940	1.934	1.959	1.909	1.931	1.942	1.967	1.944	1.952
6	1.164	1.165	1.171	1.147	1.155	1.169	1.176	1.168	1.167
7	2.275	2.269	2.278	2.230	2.235	2.278	2.287	2.271	2.260
Mean	1.975	1.969	1.982	1.939	1.954	1.976	1.990	1.975	1.975
SD	0.415	0.411	0.413	0.403	0.406	0.413	0.415	0.411	0.411

LGP: Leksell Gamm Plan, SW: solid water, PS: polystyrene, SD: standard deviation.

less than 1.1% (LGP, Leksell Gamma Plan, Elekta AB, Stockholm, Sweden). Before msr corrections were applied, the dose rates of T31010 in the polystyrene phantom were 0.70 (0.29)% higher on average than those in the SW phantom ($p = 0.018$). The A16 dose rates were 0.76 (0.32)% higher in the polystyrene phantom than in the SW phantom ($p = 0.018$). After the msr correction factors were applied, there was no statistically significant difference in the A16 dose rates measured in each phantom ($p = 0.734$), but the T31010 dose rates were 0.72 (0.29)% higher in the polystyrene phantom than in the SW phantom ($p = 0.018$). Applying msr correction factors reduced the mean value of the standard deviation between the two chambers from 1.06 (0.14)% to 0.12 (0.07)% in the SW phantom. This value was reduced from 1.02 (0.20)% to 0.53 (0.20)% in the polystyrene phantom. There was no statistically significant difference between the T31010 and A16 chambers in the SW phantom ($p = 0.351$); however, the T31010 dose rates were 0.75 (0.28)% higher than the A16 dose rates in the polystyrene phantom ($p = 0.018$).

3.3. Dose profile

Eighty films from the seven sites were analyzed to determine the FWHM and penumbra of the msr field of the Perfexion/Icon GKs. Fig. 3 shows examples of one-dimensional dose distributions along the three axes measured in the polystyrene phantom. The mean and standard deviations of the measured FWHM and penumbra are given in Table 4. The FWHM and penumbra of the dose distribution of the TMR10 algorithm of LGP version 11.3.2 are also provided. When the dose distributions obtained in the SW and polystyrene phantoms were compared, no significant differences between the two phantoms were observed ($p \geq 0.064$), except for the penumbra in the Y-axis. The penumbra in the Y-axis was wider in the polystyrene phantom than in the SW phantom ($p = 0.028$), but the difference was smaller than the variations among different sites. Both plastic phantoms provided narrower FWHMs in the XY plane than LGP.

4. Discussion

The polystyrene phantom proposed in this study showed dosimetric performance comparable to that of an SW phantom. The full width at half maximum in all directions and the penumbras in the X and Z axes were statistically equivalent in the two phantoms. The difference in the penumbra in the Y axis was smaller than the variations among GK sites. After the msr correction factors were applied, the T31010 chamber in the SW phantom and the A16 chamber in both phantoms provided statistically equivalent dose rates ($p = 0.618$). The T31010 dose rates in the polystyrene phantom were higher than the other dose rates ($p = 0.004$) because the mean msr correction factors for the T31010 chamber were the same in both phantoms, while the correction factors of the A16 chamber were 0.7% smaller in the SW phantom than in the polystyrene phantom. Since the radio-physical characteristics of solid water and polystyrene are different, different msr correction factors should be applied.

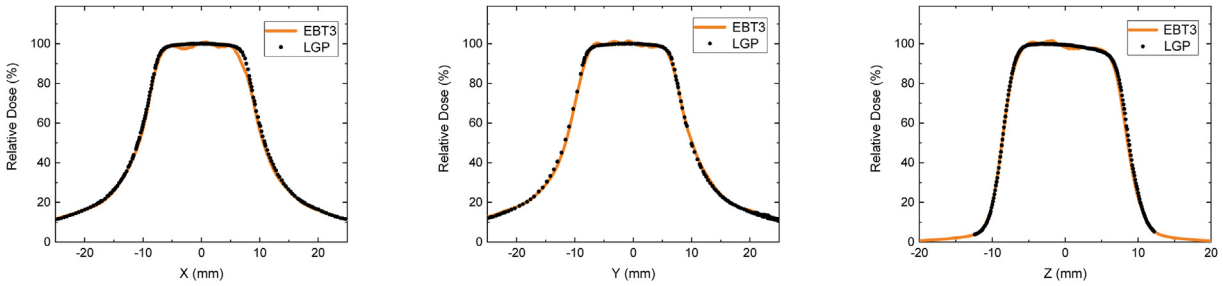

Fig. 3. One-dimensional dose profile along the three axes of the Leksell coordinate system. The solid lines are the values measured with EBT3 films in the polystyrene phantom, and the black circles are the values from the TMR 10 algorithm of Leksell Gamma Plan version 11.3.2.

Table 4
The full width at half maximum (FWHM) and penumbra of the one-dimensional dose distributions of the 16 mm collimator field of a Gamma Knife Perfexion/Icon. The values measured in the solid water and polystyrene phantoms and those calculated with the TMR10 algorithm of the treatment planning program Leksell Gamma Plan (LGP) version 11.3.2 are given.

(unit: millimeter)

	FWHM			Penumbra		
Axis	LGP	Solid water	Polystyrene	LGP	Solid water	Polystyrene
X	21.8	21.1 (0.3)	21.0 (0.2)	9.0	8.7 (0.4)	9.0 (0.4)
Y	21.8	21.2 (0.2)	21.3 (0.2)	9.0	8.7 (0.3)	8.9 (0.4)
Z	17.4	17.2 (0.1)	17.3 (0.1)	2.6	2.7 (0.1)	2.8 (0.1)

In addition to lower costs, the polystyrene phantom has several advantages over the SW phantom. First, the polystyrene phantom was designed to remove air space near the detector. As shown in Fig. 4, there is an air hole on top of the ion chamber in the chamber insert of the SW phantom. Additionally, conic air space and a larger hole are drilled to the top of the phantom. Moreover, the air gap between the chamber insert and the main phantom has non-negligible isodose surfaces because the diameter of a chamber insert is similar to the 50% isodose diameter of the msr field. In contrast, there is no air space around the chamber in the case of the polystyrene phantom. An air hole with a diameter of 1 mm was drilled from the inner phantom to the top of the polystyrene phantom, as shown in Fig. 2d and f, but this air hole was sufficiently far from the msr field. More exact dose rates to water can be obtained with the polystyrene phantom because the surrounding environment is more homogeneous. Furthermore, physicists can roughly determine whether the detector is at the correct location in the polystyrene phantom because the phantom is transparent. Additionally, as shown in Fig. 1f, the cable holder keeps the ion chamber firmly fixed during measurements, while there is no cable holder with the SW phantom.

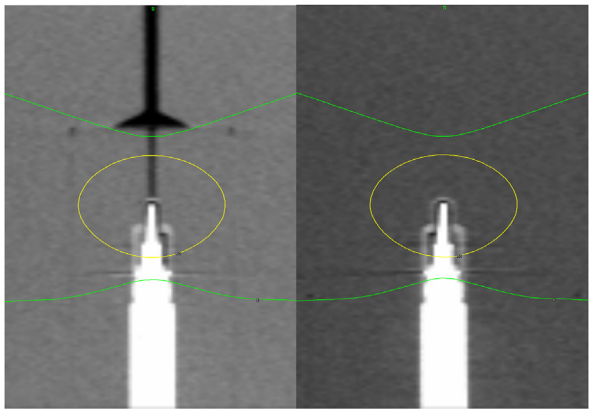

Fig. 4. Coronal cone beam CT images of a PTW T31010 ion chamber in the solid water phantom (left). There is a hole with a diameter of approximately 1 mm over the chamber. Near the chamber holder, there is a conic air space that is approximately 3 mm high and 11 mm wide. Additionally, a top hole with a diameter of approximately 2 mm was drilled to the top end. There is no air space near the chamber in the polystyrene phantom (b). The inner lines indicate the 50% isodose line, and the outer lines represent the 5% line of the 16 mm collimator field.

The polystyrene phantom performed better than the previously reported PMMA phantom [9]. While the dose rate measured in the PMMA phantom was 1.8% higher than that measured in the SW phantom, the A16 dose rates were equivalent, and the T31010 dose rates were 0.72 (0.29)% higher in the polystyrene phantom. With the PMMA phantom, the penumbras were broader than those with the SW phantom, and the differences were significant when compared with experimental uncertainties. However, the penumbras with the polystyrene phantom were nearly equivalent to those with the SW phantom. These enhancements occurred because the electron density of polystyrene is similar to that of water.

Though the polystyrene phantom of this study showed comparable characteristics to the commercial SW phantom, there are some disadvantages. The water equivalence of the electron density is poorer than the SW phantom because the electron density is more different from the electron density of water than the SW phantom. Also, the density of polystyrene varies slightly depending on the manufacturer and time of manufacture, so it is essential to measure the density and factor it into the simulation.

5. Conclusions

A polystyrene phantom was developed for gamma knife dosimetry, showing dosimetric performance comparable to a commercial solid water phantom. The absorbed dose rates to water measured using two ion chambers were nearly equivalent in both phantoms after applying machine-specific reference correction factors. The full widths at half maximum and penumbras were also consistent. However, more exact simulations of the msr correction factors for the polystyrene phantom are necessary. It is believed that more accurate simulation can be achieved by using a more extensive list of low-energy physics and detailed characteristics of

the reference field. As an extension of this research, it is likely to improve the characteristics of the current polystyrene phantom by manufacturing a phantom with much narrower air gaps.

Declaration of competing interest

The authors declare that they have no known competing financial interests or personal relationships that could have appeared to influence the work reported in this paper.

Acknowledgment

The Innopolis Foundation of Korea supported this study, funded by the Ministry of Science and ICT (Grant No. 1711149774).

References

[1] C. Lindquist, I. Paddick, The Leksell gamma Knife Perfexion and comparisons with its predecessors, Oper Neurosurg 61 (Suppl) (2007), https://doi.org/10.1227/01.neu.0000289726.35330.8a. ONS–130.
[2] M. Zeverino, M. Jaccard, D. Patin, N. Ryckx, M. Marguet, C. Tuleasca, et al., Commissioning of the Leksell gamma Knife® Icon, Med. Phys. 44 (2017) 355–363, https://doi.org/10.1002/mp.12052.
[3] H.T. Chung, Y. Park, S. Hyun, Y. Choi, G.H. Kim, D.G. Kim, et al., Determination of the absorbed dose rate to water for the 18-mm helmet of a gamma knife, Int J Radiat Oncol Biol Phys* *Biology* *Physics* 79 (2011) 1580–1587, https://doi.org/10.1016/j.ijrobp.2010.05.039.
[4] H. Palmans, P. Andreo, M.S. Huq, J. Seuntjens, K.E. Christaki, A. Meghzifene, Dosimetry of small static fields used in external photon beam radiotherapy: summary of TRS-483, the IAEA–AAPM international Code of Practice for Reference and relative dose determination, Med. Phys. 45 (2018), e1123, https://doi.org/10.1002/mp.13208. 45-e1145.
[5] P.L. Petti, M.J. Rivard, P.E. Alvarez, G. Bednarz, J. Daniel Bourland, L.A. DeWerd, et al., Recommendations on the practice of calibration, dosimetry, and quality assurance for gamma stereotactic radiosurgery: report of AAPM Task Group 178, Med. Phys. 48 (2021) e733–e770, https://doi.org/10.1002/mp.14831.
[6] Unintended attenuation in the Leksell Gamma Knife Perfexioncalibration-phantom adaptor and its effect on dose calibration, Jagdish P Bhatnagar et al. Med Phys (2009), https://doi.org/10.1118/1.3093240.
[7] J.H. Park, J.H. Han, C.Y. Kim, C.W. Oh, D.H. Lee, T.S. Suh, et al., Application of the gamma evaluation method in gamma Knife film dosimetry, Med. Phys. 38 (2011) 5778–5787, https://doi.org/10.1118/1.3641644.
[8] V. Sarkar, L. Huang, Y.J. Huang, M.W. Szegedi, P. Rassiah-Szegedi, H. Zhao, B.J. Salter, Head to head comparison of two commercial phantoms used for SRS QA, J. Radiosurg. SBRT 4 (3) (2016) 213–223. https://www.ncbi.nlm.nih.gov/pubmed/29296446.
[9] J.P. Chung, Y.M. Seong, T.Y. Kim, Y. Choi, T.H. Kim, H.J. Choi, et al., Development of a PMMA phantom as a practical alternative for quality control of gamma knife® dosimetry, Radiat. Oncol. 13 (2018) 176, https://doi.org/10.1186/s13014-018-1117-8.
[10] J. Seco, P.M. Evans, Assessing the effect of electron density in photon dose calculations, Med. Phys. 33 (2006) 540–552, https://doi.org/10.1118/1.2161407.
[11] Y. Choi, K.J. Chun, E.S. Kim, J.B. Bahng, H.J. Yang, T.H. Kim, et al., Consistency of dose rates after applying machine-specific reference correction factors for the gamma knife 16mm collimator field, Med. Phys. (2023) 1–9, https://doi.org/10.1002/mp.16242.
[12] L. Mirzakhanian, H. Benmakhlouf, F. Tessier, J. Seuntjens, Determination of factors for ion chambers used in the calibration of Leksell gamma Knife Perfexion model using EGSnrc and PENELOPE Monte Carlo codes, Med. Phys. 45 (2018) 1748–1757, https://doi.org/10.1002/mp.12821.
[13] E. Zoros, A. Moutsatsos, E.P. Pappas, E. Georgiou, G. Kollias, P. Karaiskos, et al., Monte Carlo and experimental determination of correction factors for gamma knife perfexion small field dosimetry measurements, Phys. Med. Biol. 62 (2017) 7532–7555, https://doi.org/10.1088/1361-6560/aa8590.
[14] T. Schaarschmidt, T.H. Kim, Y.K. Kim, H.J. Yang, H.T. Chung, GEANT4-based Monte Carlo simulation of beam quality correction factors for the Leksell gamma Knife® Perfexion, J. Kor. Phys. Soc. 73 (2018) 1814–1820, https://doi.org/10.3938/jkps.73.1814.
[15] T. Schaarschmidt, GEANT4-based Monte Carlo Simulation of Beam Quality Correction Factors for the Leksell Gamma Knife® Perfexion™, Thesis for the Doctor of Philosophy, 2019.
[16] A. Niroomand-Rad, C.R. Blackwell, B.M. Coursey, K.P. Gall, J.M. Galvin, W.L. McLaughlin, et al., Radiochromic film dosimetry: recommendations of AAPM radiation therapy committee task group 55. American Association of Physicists in Medicine, Med. Phys. 25 (1998) 2093–2115, https://doi.org/10.1118/1.598407.